Planetary and Space Science 122 (2016) 94–100

Contents lists available at ScienceDirect

Planetary and Space Science

journal homepage: www.elsevier.com/locate/pss

Orbit determination and gravity field recovery from Doppler tracking data to the Lunar Reconnaissance Orbiter

Andrea Maier [1], Oliver Baur [2]

Space Research Institute of the Austrian Academy of Sciences, Schmiedlstrasse 6, 8042 Graz, Austria

ARTICLE INFO

Article history:
Received 5 July 2015
Received in revised form
17 January 2016
Accepted 20 January 2016
Available online 28 January 2016

Keywords:
Precise orbit determination
Lunar gravity field
Lunar Reconnaissance Orbiter

ABSTRACT

We present results for Precise Orbit Determination (POD) of the Lunar Reconnaissance Orbiter (LRO) based on two-way Doppler range-rates over a time span of ~13 months (January 3, 2011 to February 9, 2012). Different orbital arc lengths and various sets of empirical parameters were tested to seek optimal parametrization. An overlap analysis covering three months of Doppler data shows that the most precise orbits are obtained using an arc length of 2.5 days and estimating arc-wise constant empirical accelerations in along track direction. The overlap analysis over the entire investigated time span of 13 months indicates an orbital precision of 13.79 m, 14.17 m, and 1.28 m in along track, cross track, and radial direction, respectively, with 21.32 m in total position. We compare our orbits to the official science orbits released by the US National Aeronautics and Space Administration (NASA). The differences amount to 9.50 m, 6.98 m, and 1.50 m in along track, cross track, and radial direction, respectively, as well as 12.71 m in total position. Based on the reconstructed LRO orbits, we estimated lunar gravity field coefficients up to spherical harmonic degree and order 60. The results are compared to gravity field solutions derived from data collected by other lunar missions.

1. Introduction

Lunar exploration from space started in 1966 with the launch of the lunar orbiter mission Luna-10. Further satellites of the Luna program followed, as well as the Lunar Orbiters, subsatellites of Apollo missions (Apollo 15, 16, 17), and Clementine. Lunar Prospector (LP), launched in 1998, orbited the Moon at low altitudes (30–100 km) allowing for the first time the construction of detailed gravity field models (Konopliv et al., 2001). In general, lunar gravity field recovery is severely hampered by the 1:1 spin-orbit resonance of the Earth-Moon system since direct tracking over the lunar farside is impossible. The Japanese Selenological and Engineering Explorer (SELENE), launched in 2007, provided the first global data set of the Moon by incorporating three satellites: a main orbiter in a circular orbit and two sub-satellites in elliptical orbits (Namiki et al., 1999). In addition to classical radiometric tracking data, four-way Doppler tracking between a ground station, the main orbiter, and a subsatellite was employed as well as Very Long Baseline Interferometry (VLBI) between the sub-satellites and two ground stations (Goossens et al., 2011; Kikuchi et al., 2009). In 2011, the Gravity Recovery and Interior Laboratory (GRAIL) mission was launched. By means of low-low satellite-to-satellite tracking between two spacecraft in the same orbit, an unprecedented resolution of the lunar gravity field could be achieved (Zuber et al., 2013).

The Lunar Reconnaissance Orbiter (LRO) was launched in June 2009 by the National Aeronautics and Space Administration (NASA) to prepare for future human exploration. The Lunar Orbiter Laser Altimeter (LOLA) is one of seven instruments aboard LRO (see Chin et al., 2007 for more details). LOLA determines the shape of the Moon by measuring the range from the spacecraft to the lunar surface using five beams with a nominal accuracy of 10 cm (Smith et al., 2010). To take maximum advantage of LOLA's precision the radial component of the orbit of LRO must be reconstructed to the sub-meter-level (Zuber et al., 2010); its total position has to be known within 50–100 m (e.g., Mazarico et al., 2012). During the early mapping phases LRO was orbiting the Moon in a polar, near-circular, and low altitude orbit (~50 km). This period, which lasted from September 2009 to September 2011, is hence particularly interesting for the estimation of the long wavelengths of the lunar gravity field. To keep LRO in this low-altitude orbit, Station Keeping (SK) maneuvers were performed every lunar orbit period, i.e. every 27.4 days. In addition, yaw maneuvers were undertaken every 6 months to keep LRO's single Solar Array (SA) sunlit. Every two weeks delta-H (dH) maneuvers are performed:

E-mail addresses: andrea.maier@aiub.unibe.ch (A. Maier), oliver.baur@airbus.com (O. Baur).
[1] Now at the Astronomical Institute of the University of Bern, Sidlerstrasse 5, 3012 Bern, Switzerland.
[2] Now at Airbus Defence and Space GmbH, Navigation & Apps Programmes, Robert-Koch-Str. 1, 82024 Taufkirchen, Germany.

http://dx.doi.org/10.1016/j.pss.2016.01.014
0032-0633/

LRO fires its thrusters to desaturate the momentum wheels, which absorb angular momentum caused by disturbing torques acting on the spacecraft. In December 2011, the spacecraft was moved to a quasi-frozen $\sim 30 \times 216$ km orbit (Beckman, 2006) with its perisselene over the lunar south pole to study permanently shadowed craters for water deposits. This kind of orbit gets along without SK and is thus expected to be maintained for several years (Keller et al., 2014).

In this contribution, we analyze two-way Doppler range-rates to LRO over a time span of 13 months (January 2011 to February 2012). From orbital perturbations lunar gravity field coefficients are estimated up to spherical harmonic degree and order (d/o) 60. The NASA software packages GEODYN-II (Pavlis et al., 2006) and SOLVE (Ullman, 1994) were used for Precise Orbit Determination (POD) and the estimation of lunar gravity field coefficients (see Section 3 for more details).

2. Tracking data to LRO

Due to tidal locking between the Earth and its Moon, lunar orbiters can be tracked directly only over the nearside of the Moon (cf. Fig. 1). LRO is mainly being tracked via radiometric observations at S-band (ranges and Doppler range-rates) from the primary station White Sands and from stations belonging to the Universal Space Network (USN) – see Table 1 for more details. The precision requirement of two-way range-rates was defined as 1 mm/s for the primary station and 3 mm/s for the USN stations (as shown in Section 4.1 the actual measurement noise of the range-rate observations is considerably smaller); radiometric ranges are precise to 10 m (Morinelli et al., 2010). To assist POD of the spacecraft from radiometric observations, highly accurate one-way optical laser ranging has been performed. NASA's Next Generation Satellite Laser Ranging (NGSLR) station is the primary laser tracking station. Moreover, the International Laser Ranging Service (ILRS) network (Pearlman et al., 2002) participates in tracking (see Table 2 for a list of stations). The Normal Points (NPs), which are formed from the full-rate laser data, have a nominal precision of 10 cm (Smith et al., 2008). The involvement of two non-synchronous clocks (one at the ground station and one aboard the spacecraft) imposes a bias and a drift on the measured one-way laser ranges (see Fig. 2 for an example). During the one-year nominal mission phase (September 15, 2009 to September 15, 2010), there are about six times more Doppler observations available than laser ranges (cf. Figure S1 for a comparison between Doppler and laser tracking).

For POD of LRO, we analyzed two-way Doppler range-rates on the one hand and one-way laser ranges on the other hand. The quality of laser-based orbits was, however, distinctly lower compared to Doppler-based orbits. The orbits inferred from laser ranges are discussed in Section 5. Note that radiometric ranges were not considered due to the rather poor nominal precision given above.

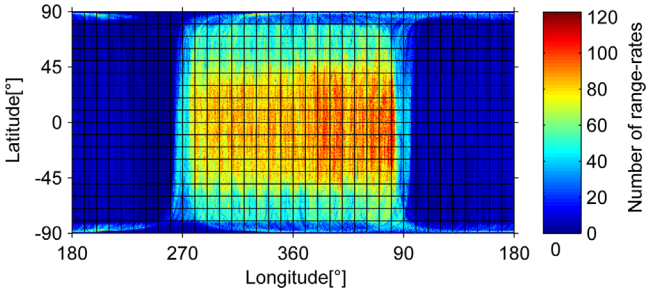

Fig. 1. Total number of Doppler range-rate measurements to LRO during the investigated time span (January 3, 2011 to February 9, 2012), averaged over a $1^\circ \times 1^\circ$ grid. The western limb of the Moon as seen from the Earth is located at 270°. (For interpretation of the references to color in this figure caption, the reader is referred to the web version of this paper.)

Table 1
Stations performing Doppler range-rate measurements to LRO.

Code	ID	Location
WS1S	119	White Sands, New Mexico, US
USPS	103	Dongara, Australia
USHS	105	South Point, Hawaii, US
KU1S, KU2S	126, 127	Kiruna, Sweden
WU1S, WU2S	128, 129	Wilheim, Germany

Table 2
Stations performing laser ranging measurements to LRO. NASA's NGSLR station is designated GO1L.

Code	ID	Location
MDOL	7080	McDonalds, Texas, USA
YARL	7090	Yarragadee, Australia
GODL	7105	Greenbelt, Maryland, USA
MONL	7110	Monument Peak, California, USA
GO1L	7125	Greenbelt, Maryland, USA
HARL	7501	Hartebeesthoek, South Africa
ZIML	7810	Zimmerwald, Switzerland
HERL	7840	Herstmonceux, United Kingdom
GRSM	7845	Grasse, France
WETL	8834	Wettzell, Germany

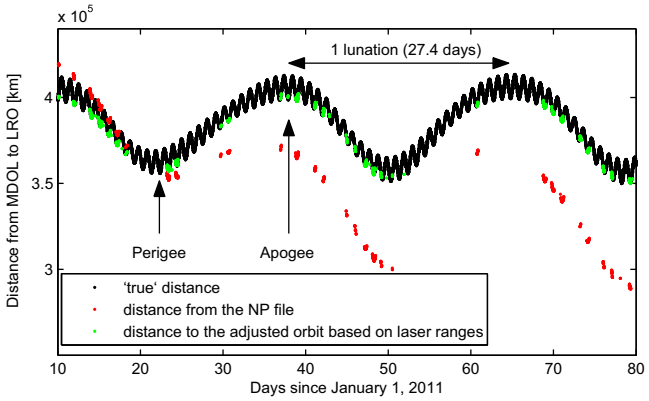

Fig. 2. The 'true' distance between McDonalds, Texas, and LRO (black color) was computed based on the science orbits, which are available at http://imbrium.mit.edu/LRORS/DATA/SPK/ in the SPICE container format. Since LRO was orbiting the Moon at only 50 km above the lunar surface for the time span shown above, the distance between the Earth and LRO is roughly the same as the distance between the Earth and the Moon (varying between ~360 000 km at perigee and ~400 000 km at apogee). Further, the one-way runtime measurements of the laser signal emitted from McDonald's, which are given in the Normal Point (NP) files, were converted to one-way distances (red color). The non-synchronous clocks at the ground station and at the spacecraft impose a bias and a drift to the range measurements. The estimation of LRO clock parameters during the orbit determination procedure based on laser ranges corrects the observed distances to realistic values (green color). (For interpretation of the references to color in this figure caption, the reader is referred to the web version of this paper.)

3. Precise orbit determination

The first step of the parameter estimation process using GEODYN consists of solving for all local or arc-specific parameters. Since the reference solution is generally not very close to the true solution, several iterations are required. Within this first step the global parameters are fixed to their a priori values. Once this system has converged, normal equations for local and global

Table 3
POD standards for LRO.

	Standard/model	Reference
Reference frame		
Inertial reference system	ICRF	McCarthy and Petit (2004)
EOPs	IERS 08 C04	Bizouard and Gambis (2007)
Planetary ephemeris	JPL DE-421	Folkner et al. (2009)
Precession-nutation model	IAU-2000	Capitaine et al. (2003)
Station coordinates	NGSLR: retrieved from the PDS[a]	
	ILRS stations: SLRF2008	Pavlis (2009)
	WS1S and USN stations: retrieved from the PDS[a]	
Gravitational force models		
Gravity field model	GL0660B (up to d/o 270)	Konopliv et al. (2013)
Solid Moon tides	IERS	McCarthy and Petit (2004)
	lunar Love number $k_2 = 0.02405$	Konopliv et al. (2013)
Third bodies	Positions: JPL DE-421	Folkner et al. (2009)
Oblateness	Direct acceleration of LRO due to Earth's oblateness	Moyer (1971)
	indirect acceleration of the Moon due to Earth's and Moon's oblateness	
Relativistic corrections	Schwarzschild, Coriolis	
Non-gravitational force models		
Solar radiation pressure	$G_0 = 1372.54\ \mathrm{Wm}^{-2}$ at 1 AU; conical shadow model	
Lunar radiation pressure	Albedo and emissivity: DLAM (d/o 15)	Floberghagen et al. (1999)
Satellite parameters		
Macro-model	10-plate macro-model given by area, normal unit vector, specular and diffuse reflectivity	Smith et al. (2008)
	Orientation of spacecraft bus, HGA, and SA derived from quaternions	
Mass	Interpolated from small forces files[b]	
Measurement models		
Tropospheric refraction	Hopfield model	Hopfield (1969)
Antenna offset[c]	(0.3, −0.3, −2.5)	
Center of mass offset[d]	(1.35, 0.00, 0.00)	
Relativistic correction	Applied	
Station displacement		
Solid Earth tide loading	IERS	McCarthy and Petit (2004)

[a] http://pds.nasa.gov/ds-view/pds/viewInstrumentProfile.jsp?INSTRUMENT_ID=RSS&INSTRUMENT_HOST_ID=LRO.
[b] http://pds-geosciences.wustl.edu/lro/lro-l-rss-1-tracking-v1/lrors0001/data/sff/.
[c] Coordinates of antenna w.r.t. the center of figure in (m); retrieved from the dimensional layouts in Tooley (2006).
[d] Coordinates of center of mass w.r.t. the center of figure in (m); retrieved from the dimensional layouts in Tooley (2006).

parameters are set up. A companion program to GEODYN, SOLVE, can now be used to stack the normal equations of several arcs and estimate the global parameters. This is achieved by reducing the normal equation system of local and global parameters by the arc-specific part. Correlations between global and arc parameters are thus taken into account. GEODYN was used in numerous previous POD and gravity field estimation work both inside the author's institution (e.g., Maier et al., 2012 for estimating the low-degree gravity field coefficients of the Earth from satellite laser ranging data) and outside (see, e.g., Lemoine et al., 2001 for Mars and Mazarico et al., 2012 for the Moon).

Relevant information for LRO orbit modeling such as reference frame, gravitational and non-gravitational force models, satellite parameters, and measurement standards is summarized in Table 3. The gravity field model GL0660B (Konopliv et al., 2013), which was derived from the Gravity Recovery and Interior Laboratory (GRAIL) mission, served as a priori gravity field model. To find a suitable truncation level from the viewpoint of computational costs, a forward integration was made over a time span of six months using (1) maximum d/o 270 and (2) maximum d/o 540 as truncation levels. The Root Mean Square (RMS) values of orbit differences between the two integration results are 0.66 m, 0.55 m, and 0.08 m in along track, cross track, and radial direction, respectively, and 0.86 m in total position. Recalling LRO's position accuracy requirements (cf. Section 1), truncating the a priori gravity field at d/o 270 seems to be a suitable tradeoff between orbital precision and computing time.

Laser ranges and Doppler measurements refer to the tracking point at the High Gain Antenna (HGA), and must therefore be transferred to the center of mass (see Table 3). The shape of LRO is approximated by a macro-model consisting of ten flat plates: six plates for the spacecraft bus, two plates for the SA, and two plates for the HGA. Each plate is characterized by a unit normal vector, a plate area, and specular and diffuse reflectivity coefficients (Smith et al., 2008). The orientation of the three components of LRO's macro-model, i.e. spacecraft bus, SA, and HGA, was retrieved from the Planetary Data System (PDS).[3] Using the Spacecraft Planet Instrument C-matrix Events (SPICE)[4] information system within the MATLAB environment, which is provided by NASA's Navigation and Ancillary Information Facility (NAIF), the pointing data were converted from transformation matrices to unit quaternions.[5] The three sets of quaternions relate (1) the LRO spacecraft frame to the Moon mean equator and equinox of date reference frame (J2000), (2) the SA frame to the spacecraft frame, and (3) the HGA frame to the spacecraft frame. The acceleration due to non-gravitational forces acting on LRO, such as solar radiation pressure, is thus the sum of the accelerations acting on each individual plate. For more details about non-gravitational force modeling the reader is referred to Table 3.

[3] ftp://naif.jpl.nasa.gov/pub/naif/pds/data/lro-l-spice-6-v1.0/lrosp_1000/data/ck/.
[4] http://naif.jpl.nasa.gov/naif/.
[5] A quaternion is a four-component representation of a rotation matrix: one component is a scalar describing the angle of rotation and the remaining three components specify the rotation axis; a unit quaternion has a magnitude of one.

Table 4
Estimated parameters for POD based on Doppler range-rates.

Arc parameters	
Initial state	
Solar radiation pressure coefficient	1 per arc
Empirical acceleration	Along track constant (1 per arc)
Measurement bias	1 per station and arc
Satellite state vector	1 per arc
Global parameters	
Gravity field coefficients	Up to d/o 60

3.1. Seeking the optimal parametrization

Orbit accuracy can only be as good as orbit precision. To assess the latter, orbit overlap tests were conducted over three science mission phases, SM05 to SM07, lasting from January 3, 2011 to March 27, 2011. The objective was to find (1) the optimal set of empirical accelerations and (2) the optimal arc length. All tests are based solely on Doppler range-rates since this is the major measurement type. In addition to orbit overlaps, observation residuals were analyzed. Concerning the estimation of empirical accelerations, the following five scenarios were tested:

- along track constant,
- along track 1-cycle per revolution (1-cpr),
- along track constant and along track 1-cpr,
- along track constant and cross track constant,
- along track constant and cross track 1-cpr.

Further, three different arc lengths were evaluated: an arc length of l.25 days (short arcs), an arc length of 2.5 days (medium arcs), and an arc length of 4.5 days (long arcs). Short, medium, and long arcs overlap by 6 h, 12 h, and 36 h, respectively (cf. Figure S2).

In case of short arcs, the RMS value of overlap differences amounts to 25.64 m in total position when estimating one constant empirical parameter in along track direction (Table S1). The overall RMS value of the residuals (3.9 mm/s) is larger than the nominal precision (1 mm/s for WS1S and 3 mm/s for the USN stations). Figure S3 (left) reveals, however, that the large RMS value of the residuals comes from a few very large residuals. For time spans when these large residuals are missing, the residuals of the short arcs are smaller than those of the medium arcs (cf. Figure S3, right). Due to the large orbit overlap differences compared to medium arcs, the short arcs were not further investigated. The residuals of the medium arcs are more homogenous compared to the short arcs (cf. Figure S3, left). Among all five scenarios of empirical accelerations listed above, estimating a constant empirical acceleration in along track direction yields the smallest RMS value of overlap differences in total position, i.e. 3.57 m (cf. Table S2). For long arcs the RMS values of overlap differences and residuals tend to increase compared to medium arcs (Table S3).

The analysis of orbit overlaps and observation residuals revealed that the highest precision is achieved by using an arc length of 2.5 days and by estimating one constant empirical acceleration per arc in along track direction. Note that in addition to the LRO simulation performed by Rowlands et al. (2009), Mazarico et al. (2012) presented and used this exact strategy (2.5 days, constant acceleration in along-track direction) for orbit reconstruction. The optimal arc length and the optimal choice of empirical accelerations have been adopted for all further investigations.

The nominal precision of the primary station's tracking data is by a factor of 3 better compared to the USN stations (cf. Section 2). Hence, one would expect that assigning a standard deviation of

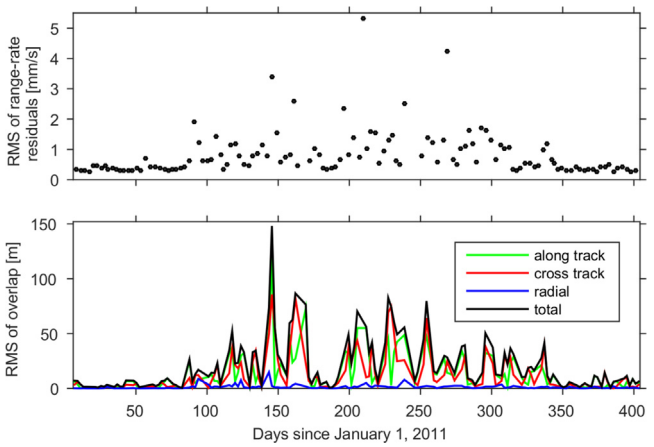

Fig. 3. RMS values of Doppler range-rate residuals per arc (top) and RMS values of orbit overlap differences per overlap (bottom). (For interpretation of the references to color in this figure caption, the reader is referred to the web version of this paper.)

1 mm/s to the observations of the primary station and 3 mm/s to those of the USN stations would result in more precise orbits than using the same standard deviation for all observations. This was, however, not the case. Computing RMS values of the Doppler range-rate residuals averaged over all arcs (13 months) for the primary station on one hand and for the secondary stations on the other hand gave an RMS value of 0.72 mm/s for the primary station and 0.82 mm/s for the USN stations. Hence, the performance of primary and secondary stations is much more alike than the nominal values would suggest.

4. Results

4.1. POD

We analyzed about 13 months of Doppler data (January 3, 2011 to February 9, 2012) to LRO, which relate to 15 science mission phases (SM05 to SM19). To assess orbital precision, the time span of 13 months was subdivided into overlapping arcs of 2.5 days; two consecutive arcs overlap by 12 h. Estimated arc parameters and global parameters are summarized in Table 4. The range-rate residuals, which are the differences between the observed and the computed range-rates, are an indicator for the precision of orbit modeling. Fig. 3 (top) shows that for the vast majority of the orbital arcs the RMS values of the range-rate residuals are considerably smaller than the precision requirement (i.e. 1 mm/s for the primary station and 3 mm/s for all other stations). Fig. 3 (bottom) depicts the RMS values of the orbit overlap differences with respect to the spacecraft reference frame (i.e. in along track, cross track, and radial direction). Over the entire investigated time span, the overlap tests indicate that the orbit determined from Doppler range-rates is precise to 13.79 m, 14.17 m, and 1.28 m in along track, cross track, and radial direction, respectively, with 21.32 m in total position.

Both the RMS of range-rate residuals and the RMS of orbit overlaps (cf. Fig. 3) show smaller values at the beginning and at the end of the investigated period. Park et al. (2012) states that for smaller solar beta angles[6] the modeling of non-gravitational forces becomes more difficult as the perturbations are changing more rapidly due to part of the orbit being in shadow. During the investigated time span the solar beta angle is at its maximum (i.e.

[6] The solar beta angle is the angle between the orbital plane and the Sun.

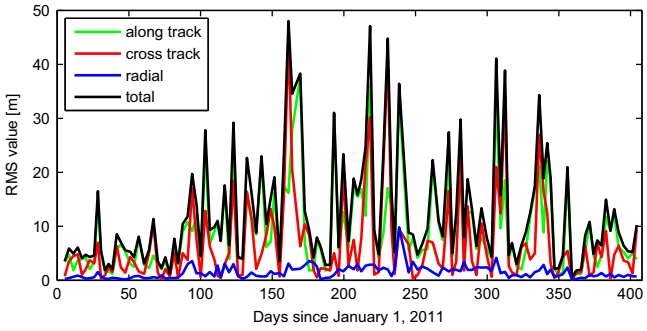

Fig. 4. RMS values of differences per arc between the LRO orbit presented in this study (based on Doppler range-rates only) and the science orbit as computed by NASA (based on Doppler range-rates, radiometric ranges, and altimetric crossovers). (For interpretation of the references to color in this figure caption, the reader is referred to the web version of this paper.)

90° or −90°) around day 1, day 170, and day 350 of 2011. Whereas the values are indeed small during the first and third maximum, they are much larger during the second one. Hence, a correlation between orbital precision and the solar beta angle cannot be clearly identified.

We externally validated our estimated LRO orbits by comparison with the science orbits[7] produced by the The Lunar Orbiter Laser Altimeter (LOLA) team (cf. Fig. 4). One has to keep in mind, though, that the tracking data the orbits are based on are not the same. Whereas for this study solely Doppler measurements were used, the science orbits additionally incorporate radiometric ranges and altimetric crossovers (Mazarico et al., 2012). The RMS values of the orbit differences are 9.50 m, 6.98 m, and 1.50 m in along track, cross track, and radial direction, respectively, with 12.71 m in total position.

Figure S4 compares the magnitude of the gravitational accelerations acting on LRO. Third bodies and the solid Moon tides have the largest impact. The acceleration due to solar and lunar radiation pressure is shown in Figure S5 for a low and a high solar beta angle.

4.2. Gravity field

For the estimation of the lunar gravity field (in terms of spherical harmonic coefficients) we re-computed the orbit without overlapping periods. The arc length is approximately 3 days including on average 18 White Sands passes as well as passes from secondary stations. Over the entire investigated time span of 13 months, all orbital arcs were combined for the determination of gravity field coefficients up to d/o 60. In total, our gravity field solution is based on ∼1 900 000 Doppler range-rates.

The farside data gap (cf. Fig. 1) considerably hampers the computation of global gravity field models. Hence, we applied Tikhonov–Phillips regularization (Tikhonov, 1963; Phillips, 1962) to overcome the ill-posedness of the inversion process. The Tikhonov–Phillips regularized version of a normal equation system reads $\hat{\mathbf{x}}_\eta = \left(\mathbf{A}^T\mathbf{P}\mathbf{A}+\eta\mathbf{K}\right)^{-1}\mathbf{A}^T\mathbf{P}\mathbf{y}$, where $\hat{\mathbf{x}}_\eta$ is the estimated state deviation, $\mathbf{A}$ is the design matrix, $\mathbf{P}$ is the weight matrix, η is the regularization parameter, $\mathbf{K}$ is a symmetric regularization matrix, and $\mathbf{y}$ is the observation deviation. The regularization matrix was set up empirically according to Kaula's rule (Kaula, 1966), i.e. $\sigma_n^2 = \left(\frac{1\cdot10^{-5}}{n^2}\right)^2$ with σ_n^2 being the variances of degree n. To find the optimal regularization parameter, the L-curve criterion was adopted (e.g., Hansen, 1998, 2000). This method makes use of the

[7] Downloaded from http://imbrium.mit.edu/LRORS/DATA/SPK/

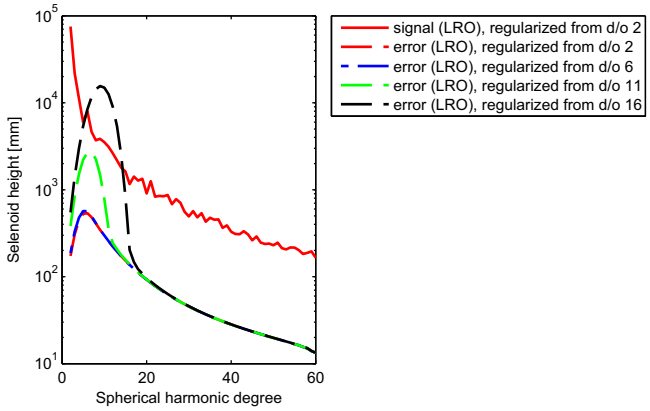

Fig. 5. Degree-wise signal and errors of the gravity field coefficients estimated from Doppler range-rates to LRO in terms of selenoid height. The formal errors are shown for solutions regularized from d/o 2, 6, 11, and 16 onwards. (For interpretation of the references to color in this figure caption, the reader is referred to the web version of this paper.)

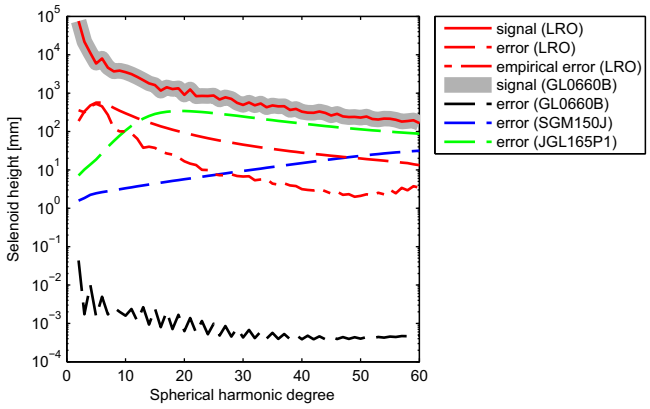

Fig. 6. Degree-wise signal, formal errors, and empirical errors (w.r.t. GL0660B) of the recovered gravity field solution based on Doppler range-rates to LRO in terms of selenoid height (in red color). In addition, the signal and the errors of the a priori GRAIL-derived model (GL0660B) are shown. Further, the errors of JGL165P1 (based on LP data) and those of SGM150J (based on LP and SELENE data) are depicted. (For interpretation of the references to color in this figure caption, the reader is referred to the web version of this paper.)

solution norm and the residual norm:

$$\left\{\underbrace{\|\mathbf{y}-\mathbf{A}\mathbf{x}\|_{\mathbf{P}}^2}_{\text{residual norm}}+\eta\ \underbrace{\|\mathbf{x}_\eta\|_{\mathbf{K}}^2}_{\text{solution norm}}\right\}\rightarrow\min_{\mathbf{x}}. \tag{1}$$

Plotting the solution norm against the residual norm for various a priori defined values for η results in a curve similar to an 'L'. The optimal regularization parameter, which corresponds to the point at the corner of the L-shaped curve, represents a compromise between data misfit and the power of the solution.

Four gravity field solutions were computed by regularizing all coefficients from d/o 2, 6, 11, and 16 onwards. Whereas the formal errors of the first two solutions are nearly identical (cf. Fig. 5), a significant increase of the formal errors occurs when the regularization starts at d/o 11 or 16. Whereas the power of the signal is nearly identical for the solutions regularized from d/o 2, d/o 6, and d/o 11 onwards, the coefficients show anomalous power when it comes to the solution where all coefficients from d/o 16 onwards are regularized; in this case the signal is dominated by the formal errors and it shows the same bulge as the errors (not shown here). Based on Fig. 5 the decision was made to freely adjust all

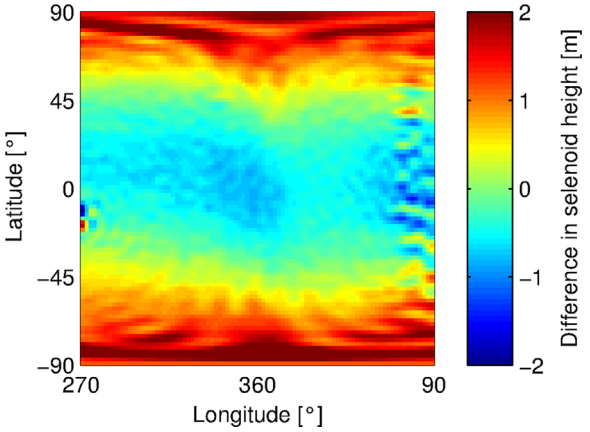

Fig. 7. Differences in selenoid height between our regularized gravity field solution (truncated at d/o 50) and the a priori gravity field model GL0660B (nearside only). (For interpretation of the references to color in this figure caption, the reader is referred to the web version of this paper.)

coefficients up to d/o 5 and starting the regularization at d/o 6; the optimal regularization parameter η (cf. Eq. (1)) for this case is equal to 9.

The signal and errors of the estimated gravity field coefficients can be compared against those of the a priori gravity field model GL0660B (Fig. 6). Whereas the signals agree well, the errors of the LRO-derived solution are significantly larger than those of GL0660B. Note that GRAIL provided a substantial leap of knowledge due to the concept of low-low satellite-to-satellite tracking (Zuber et al., 2013). Since no model is available that is solely based on tracking data to LRO, the errors of the LP-derived model JGL165P1 are shown in Fig. 6 to compare with the LRO-derived solution; this comparison is justified as JGL165P1 is also based on ground-based tracking data. Up to d/o 12, the formal errors of the LRO-based gravity field solution are larger than those of JGL165P1. We attribute this to the fact that the latter contains 18 months of radio tracking data to LP as well as historical data to the Lunar Orbiters 1 to 5, the Apollo 15 and 16 subsatellites, and to Clementine (Konopliv et al., 2001). More importantly, those different spacecraft were in a variety of orbits, in particular inclination, and hence better suited to separate correlated (lumped) coefficients than it is the case for the single-spacecraft solution presented here. The errors of JGL165P1 steadily increase up to d/o 15 since regularization was applied from d/o 16 onwards (Konopliv et al., 2001). The error level of SGM150J (Goossens et al., 2011), a SELENE-derived gravity field model including data to LP, is slightly lower compared to JGL165P1 and the LRO-derived model as tracking data are available over the lunar farside.

Assuming that the a priori gravity field model GL0660B represents the true signal, the so-called empirical error can be derived, which is simply the spectrum of differences between our solution and GL0660B (cf. Fig. 6). For the unregularized part of our solution, i.e. from d/o 2 to d/o 5, the formal and empirical errors agree well supporting the choice of the optimal regularization parameter. For the regularized part, however, the formal errors are too conservative.

Fig. 7 presents the differences in selenoid height between our regularized gravity field solution and the a priori gravity field model GL0660B for the nearside of the Moon. With at maximum ± 2 m the differences are largest at the poles were Doppler tracking is sparsest (cf. Fig. 1). At the farside of the Moon, the differences are as large as ± 15 m (not shown here).

5. Discussion

Mazarico et al. (2013) assessed the orbital precision of the LRO science orbits (as computed by NASA) via orbit overlaps. For the time span between September 2010 and December 2011, the science orbits have been reported to be precise to 8.34 m, 7.05 m, and 0.60 m in along track, cross track, and radial direction, and 10.04 m in total position. Comparing these orbits with those presented in this work yields difference RMS values of 9.50 m, 6.98 m, 1.50 m and 12.71 m in along track, cross track, radial direction and total position, respectively. These RMS values are in good agreement with the aforementioned inner precision of the LRO science orbits. We attribute the occurring differences to the exclusion/inclusion of radiometric ranges, on the one hand. On the other hand, it should be emphasized that the periods the statistics refer to are not identical but shifted by several months (January 2011 to February 2012 versus September 2010 to December 2011).

An attempt was made to determine LRO's orbit solely from laser ranges. For this purpose, we subdivided a time span of about three months (SM05 to SM07) into arcs of 7 days in length. The estimated parameters include the initial state, one solar radiation pressure coefficient per arc, one constant empirical acceleration in along track direction per arc, one measurement bias per station and pass, and one LRO clock drift rate and aging rate per arc. The RMS values between the laser-based orbits and the science orbits turned out to be 373 m, 23 m, and 17 m in along track, cross track, and radial direction, respectively. The reason for this poor precision is not yet fully understood. It might be related to deficiencies in LRO clock modeling. This suspicion, however, requires further investigation.

The authors also tried to determine LRO's orbit from laser ranges and Doppler range-rates in a combined estimation process. A series of tests has shown, however, that no convergence is achieved using the respective nominal precision, i.e. 1 mm/s for Doppler range-rates and 10 cm for laser ranges. Increasing the standard deviation for laser ranges to an unrealistically large value of $\sim$1 m results in convergence; the orbit turned out to be of much poorer quality compared to that one determined from Doppler-only data though. Increasing the standard deviation further to several meters results in an orbit similar to the Doppler-only orbit but then the laser ranges have only a tiny contribution.

6. Conclusion

We presented POD results for LRO over a time span of 13 months. Our LRO orbits, which are based solely on two-way Doppler range-rates, have an inner precision considerably higher than the original mission requirements. We externally validated our Doppler-based orbits with the official LRO science orbits (computed by NASA) that include radiometric ranges and cross-overs as well. Our orbits and those computed by NASA are in good agreement. Moreover, the RMS of the orbit differences is very similar to the inner precision of our orbits.

Acknowledgments

The software packages GEODYN-II and SOLVE were kindly provided by the NASA Goddard Space Flight Center; we are grateful to David D. Rowlands and Erwan Mazarico for technical and scientific support. The authors would like to acknowledge the comments of two anonymous reviewers.

Appendix A. Supplementary data

Supplementary data associated with this paper can be found in the online version at http://dx.doi.org/10.1016/j.pss.2016.01.014.

References

Beckman, M., 2006. Mission design for the Lunar Reconnaissance Orbiter. URL ⟨http://lunar.gsfc.nasa.gov/library/LRO_AAS_Paper_07-057.pdf⟩.

Bizouard, C., Gambis, D., 2007. The combined solution C04 for Earth orientation parameters consistent with international terrestrial reference frame 2008. URL ⟨ftp://hpiers.obspm.fr/iers/eop/eopc04/C04.guide.pdf⟩.

Capitaine, N., Wallace, P.T., Chapront, J., 2003. Expressions for IAU 2000 precession quantities. Astron. Astrophys. 412, 567–586.

Chin, G., Brylow, S., Foote, M., Garvin, J., Kasper, J., Keller, J., Litvak, M., Mitrofanov, I., Paige, D., Raney, K., Robinson, M., Sanin, A., Smith, D., Spence, H., Spudis, P., Stern, S.A., Zuber, M., 2007. Lunar Reconnaissance Orbiter overview: the instrument suite and mission. Space Sci. Rev. 129 (May (4)), 391–419.

Floberghagen, R., Visser, P., Weischede, F., 1999. Lunar albedo force modelling and its effect on low lunar orbit and gravity field determination. Adv. Space Res. 23 (4), 733–738.

Folkner, W.M., Williams, J.G., Boggs, D.H., 2009. The planetary and lunar ephemeris DE 421. Interplanetary network progress report 42-178. URL ⟨http://ipnpr.jpl.nasa.gov/progress_report/42-178/178C.pdf⟩.

Goossens, S., Matsumoto, K., Liu, Q., Kikuchi, F., Sato, K., Hanada, H., Ishihara, Y., Noda, H., Kawano, N., Namiki, N., Iwata, T., Lemoine, F.G., Rowlands, D.D., Harada, Y., Chen, M., 2011. Lunar gravity field determination using SELENE same-beam differential VLBI tracking data. J. Geod. 85 (4), 205–228.

Hansen, P.C., 1998. Rank-Deficient and Discrete Ill-Posed Problems: Numerical Aspects of Linear Inversion. Siam Monographs on Mathematical Modeling and Computation.

Hansen, P.C., 2000. The l-curve and its use in the numerical treatment of inverse problems. In: Johnston, P. (Ed.), Computational Inverse Problems in Electrocardiology. Advances in Computational Bioengineering. WIT Press, Southampton, pp. 119–142.

Hopfield, H.S., 1969. Two-quartic trophospheric refractivity profile for correcting satellite data. J. Geophys. Res. 74 (18), 4487–4499.

Kaula, W.M., 1966. Theory of Satellite Geodesy. Blaisdell Pub. Co., London.

Keller, J.W., Petro, N.E., McClanahan, T.P., Vondrak, R.R., Garvin, J.B., 2014. Recent results from the Lunar Reconnaissance Orbiter mission and plans for a second extended science mission. In: Proceedings of the 45th Lunar and Planetary Science Conference, The Woodlands, Texas. URL ⟨http://www.hou.usra.edu/meetings/lpsc2014/pdf/2294.pdf⟩.

Kikuchi, F., Liu, Q., Hanada, H., Kawano, N., Matsumoto, K., Iwata, T., Goossens, S., Asari, K., Ishihara, Y., Tsuruta, S., Ishikawa, T., Noda, H., Namiki, N., Petrova, N., Harada, Y., Ping, J., Sasaki, S., 2009. Picosecond accuracy VLBI of the two subsatellites of SELENE (KAGUYA) using multifrequency and same beam methods. Radio Sci. 44 (April (2)).

Konopliv, A., Asmar, S.W., Carranza, E., Sjogren, W.L., Yuan, D.N., 2001. Recent gravity models as a result of the lunar prospector mission. Icarus 150 (March), 1–18.

Konopliv, A.S., Park, R.S., Yuan, D.-N., Asmar, S.W., Watkins, M.M., Williams, J.G., Fahnestock, E., Kruizinga, G., Paik, M., Strekalov, D., Harvey, N., Smith, D.E., Zuber, M.T., 2013. The JPL lunar gravity field to spherical harmonic degree 660 from the GRAIL primary mission. J. Geophys. Res. Planets 118 (July (7)), 1415–1434.

Lemoine, F.G., Smith, D.E., Rowlands, D.D., Zuber, M.T., Neumann, G.A., Chinn, D.S., Pavlis, D.E., 2001. An improved solution of the gravity field of Mars (GMM-2B) from Mars Global Surveyor. J. Geophys. Res. (E10), 23,359–23,376.

Maier, A., Krauss, S., Hausleitner, W., Baur, O., 2012. Contribution of satellite laser ranging to combined gravity field models. Adv. Space Res. 49 (3), 556–565.

Mazarico, E., Goossens, S.J., Lemoine, F.G., Neumann, G.A., Torrence, M.H., Rowlands, D.D., Smith, D.E., Zuber, M.T., 2013. Improved orbit determination of lunar orbiters with lunar gravity fields obtained by the GRAIL mission. In: Lunar and Planetary Science Conference, vol. 44, p. 2414.

Mazarico, E., Rowlands, D.D., Neumann, G.A., Smith, D.E., Torrence, M.H., Lemoine, F.G., Zuber, M.T., 2012. Orbit determination of the Lunar Reconnaissance Orbiter. J. Geod. 86 (September (3)), 193–207.

McCarthy, D.D., Petit, G. (Eds.), 2004. IERS conventions (2003). IERS Technical Note No. 32. Verlag des Bundesamtes für Kartographie und Geodäsie, Frankfurt am Main 2004. URL ⟨http://202.127.29.4/cddisa/data_base/IERS/Convensions/Convension_2003/tn32_IERS_Conventions_2003.pdf⟩.

Morinelli, P.J., Socoby, J., Hendry, S., Campion, R., 2010. Tracking data certification for the Lunar Reconnaissance Orbiter. In: Proceedings of the SpaceOps 2010 Conference, Huntsville, Alabama, pp. 1–16. URL ⟨http://arc.aiaa.org/doi/pdf/10.2514/6.2010-2129⟩.

Moyer, T., 1971. Technical Report 32-1527, NASA, Jet Propulsion Lab., California Institute of Technology, Pasadena, California.

Namiki, N., Hanada, H., Tsubokawa, T., Kawano, N., Ooe, M., Heki, K., Iwata, T., Ogawa, M., Takano, T., 1999. Selenodetic experiments of SELENE: relay subsatellite, differential VLBI and laser altimeter. Adv. Space Res. 23 (11), 1817–1820.

Park, R., Asmar, S.W., Fahnestock, E.G., Konopliv, A.S., Lu, W., Watkins, M.M., 2012. Gravity Recovery and Interior Laboratory simulations of static and temporal gravity field. J. Spacecr. Rockets 49 (March (2)), 390–400.

Pavlis, D.E., Poulose, S.G., McCarthy, J.J., 2006. GEODYN operations manuals. Contractor Report, SGT Inc., Greenbelt.

Pavlis, E.C., 2009. SLRF2008: The ILRS reference frame for SLR POD contributed to ITRF2008. URL ⟨http://www.aviso.altimetry.fr/fileadmin/documents/OSTST/2009/oral/Pavlis.pdf⟩.

Pearlman, M.R., Degnan, J.J., Bosworth, J.M., 2002. The international laser ranging service. Adv. Space Res. 30 (2), 135–143.

Phillips, D.L., 1962. A technique for the numerical solution of certain integral equations of the first kind. J. ACM 9, 84–97.

Rowlands, D.D., Lemoine, F.G., Chinn, D.S., Luthcke, S.B., 2009. A simulation study of multi-beam altimetry for Lunar Reconnaissance Orbiter and other planetary missions. J. Geod. 83 (8), 709–721.

Smith, D., Zuber, M., Lemoine, F., Torrence, M., Mazarico, E., 2008. Orbit determination of LRO at the Moon. URL ⟨http://www.astro.amu.edu.pl/ILRS_Workshop_2008/presentations/1_mon/sess2/2_Smith.pdf⟩.

Smith, D.E., Zuber, M.T., Jackson, G.B., Cavanaugh, J.F., Neumann, G.A., Riris, H., Sun, X., Zellar, R.S., Coltharp, C., Connelly, J., Katz, R.B., Kleyner, I., Liiva, P., Matuszeski, A., Mazarico, E.M., McGarry, J.F., Novo-Gradac, A.-M., Ott, M.N., Peters, C., Ramos-Izquierdo, L.A., Ramsey, L., Rowlands, D.D., Schmidt, S., Scott, V.S., Shaw, G.B., Smith, J.C., Swinski, J.-P., Torrence, M.H., Unger, G., Yu, A.W., Zagwodzki, T.W., 2010. The lunar orbiter laser altimeter investigation on the Lunar Reconnaissance Orbiter mission. Space Sci. Rev. 150 (May (1–4)), 209–241.

Tikhonov, A.N., 1963. Solution of incorrectly formulated problems and the regularization method. Soviet Math. Dokl. 4, 1035–1038.

Tooley, C., 2006. Lunar Reconnaissance Orbiter spacecraft & objectives. URL ⟨http://lunar.gsfc.nasa.gov/library/tooley-scobjectives-51906.pdf⟩.

Ullman, R.E., 1994. SOLVE program: mathematical formulation and guide to user input. Hughes/stx Contractor Report, Contract nas5-31760, NASA Goddard Space Flight Center, Greenbelt, Maryland.

Zuber, M.T., Smith, D.E., Watkins, M.M., Asmar, S.W., Konopliv, A.S., Lemoine, F.G., Melosh, H.J., Neumann, G.A., Phillips, R.J., Solomon, S.C., Wieczorek, M.A., Williams, J.G., Goossens, S.J., Kruizinga, G., Mazarico, E., Park, R.S., Yuan, D.-N., 2013. Gravity field of the Moon from the Gravity Recovery and Interior Laboratory (GRAIL) mission. Science 339 (February (6120)), 71–668.

Zuber, M.T., Smith, D.E., Zellar, R.S., Neumann, G.A., Sun, X., Katz, R.B., Kleyner, I., Matuszeski, A., McGarry, J.F., Ott, M.N., Ramos-Izquierdo, L.A., Rowlands, D.D., Torrence, M.H., Zagwodzki, T.W., 2010. The Lunar Reconnaissance Orbiter laser ranging investigation. Space Sci. Rev. 150 (May), 63–80.